Gas–water distribution pattern of large-scale low and gentle structure gas reservoirs — a case study of the Longwangmiao Formation gas reservoir in MX gas field in Sichuan Basin

Peiyan Li[a], Chao Cheng[a,*], Jifu Ruan[b], Hong Luo[b], Wusheng Li[c], Yu Ye[a], Yuqiang Jiang[a], Yu Deng[a,d], Cheng Huang[a,e]

[a]*School of Geoscience and Technology, Southwest Petroleum University, Chengdu 610500, China, email: ylksh@163.com (C. Cheng)*
[b]*Central Sichuan Oil and Gas Mine, Petrochina Southwest Oil and Gas Field Company, Suining 629000, China*
[c]*Qinghai Oilfield Development Department, Petrochina Co., Ltd., Dunhuang 736202, China*
[d]*Sichuan Vocational College of Science and Technology, Meishan 620564, China*
[e]*Petrochina Western Drilling Engineering Co., Ltd., Kelamayi 834000, China*

ABSTRACT

Clarifying the gas–water distribution of gas reservoirs can effectively develop water-bearing gas reservoirs and form water control schemes. The Longwangmiao Formation gas reservoir in MX gas field in Sichuan Basin (hereinafter referred to as "Longwangmiao Reservoirs") is a large-scale gas reservoir with low and gentle structure. The current production dynamics have proved that the early understanding of uniform gas–water interface and water invasion does not reflect the reality. The special and complex storage mode and water invasion characteristics of the formation water requires detailed and accurate descriptions of the gas–water relationship and the water invasion behavior of gas reservoirs. This paper first defines the storage mode of how the formation water structures the main area of the gas reservoirs where the edge water and locally sealed water coexist the main control factors. Based on the comprehensive interpretation of oil test and logging, this paper discusses the relationship between the water saturation in water and the structural elevation of the structure to establish a water saturation-gas column height model, thus defining the optimal gas–water interface of the gas reservoirs with refined and accurate description of the original gas–water distribution pattern of gas reservoirs. This paper also reveals the water invasion behavior and the dynamic change pattern of gas–water distribution by combining the seepage-capacity-based reservoir distribution pattern with the dynamic production characteristics. The study shows that: (1) the original gas–water interface s of the gas reservoirs are not unified. The north wing of the main area is rather consistent with a changing range of –4,385 ± 3 m, while the southern wing varies greatly with a range of –4,390 ~ –4,410 m due to the influence of dip angle and water energy; (2) The Longwangmiao Reservoirs can be classified into three categories according to seepage capacity which are heterogeneous; (3) Influenced by multiple factors such as structure, lithology, pore throat structure, degree of fracture development and coexistence of various formation water storage modes, the gas–water interface does not advance uniformly and evenly during the development, while the water in the main area advances rapidly along the high permeability zone and the fracture development area of Type I reservoir.

Keywords: Longwangmiao Formation; Large-scale low and gentle structure; Gas–water relationship; Water invasion dynamics; Careful description

* Corresponding author.

1. Introduction

The discovery of Sinian–Cambrian gas reservoir in MX Block marks a breakthrough in Sichuan Basin after the finding of Weiyuan Sinian gas reservoir, among which the gas reservoir in Cambrian Longwangmiao Formation has the largest single integrated marine gas field in China [1,2]. In the Longwangmiao Formation, Dolomite reservoir with a stable thickness is widely developed where the reservoir space is dominated by dissolution pores, followed by intergranular pores and intercrystalline pores, with underdeveloped fractures [3–6]. The source rock under the Lower Cambrian Qiongzhusi Formation provides abundant gas source for the gas reservoir, while the dense carbonate rock mixed with gypsum-salt of Gaotai Formation is the immediate cap rock. The combination of source-reservoir-cap provides geological conditions for the Longwangmiao Formation in eastern Sichuan to accumulate oil and gas to the extend as large fields [7–9]. Since 2012, good indication of oil and gas has been found in several wells in the Longwangmiao Formation in the exploration for the purpose of Paleozoic–Sinian. In September 2012, the test generated 107.18×10^4 m^3/d gas in Longwangmiao Formation MX 8 in the east high point of MX Block yielded, initiating the exploration and development of the Longwangmiao Reservoirs. Since then, high yield industrial gas flow was obtained in MX9, MX10 and MX11. Through relevant research on the water-gas distribution of the Longwangmiao Reservoirs, scholars reached consensus that the gas reservoir has a uniform gas–water interface at –4,385 m [10,11]. In fact, under the influence of the formation structure, reservoir macro-physical properties, micro pore throat structure and heterogeneity, the storage mode and water invasion of the formation water in the Longwangmiao Reservoirs with a large-scale low and gentle structure are inherently special and complex. A uniform gas–water interface does not reflect the real original gas–water distribution, nor it is consistent with the actual production. For example, wells at a higher position of MX Block yield produces water while adjacent wells at a lower position still produce pure gas. Therefore, it is urgent to obtain the fine description of the gas–water distribution pattern and water invasion behavior of the gas reservoirs to provide basis for projects to develop gas reservoirs and water management control schemes efficiently.

2. Geological background

Sichuan Basin, located on the northwest edge of Yangtze Platform, is a typical multi-stage tectonic superimposition basin evolved through polycyclic development [12,13]. The Longwangmiao Reservoirs is located in Weiyuan ~ Longnvsi in the paleouplift gentle structure group of Sichuan Basin, with Guang'an structure in the east, Weiyuan structure in the west, Penglai Town structure in the north, Hebaochang and Jieshichang buried structure in the southwest, and the high-steep structure area in the southeast of Sichuan, as shown in Fig. 1. The paleouplift in central Sichuan was formed in as early as the sedimentary period when the Sinian Dengying Formation developed, forming the paleo-geographical pattern where the west and south are higher, while the east and north part are lower. When it comes to the early Cambrian Canglangpu sedimentary period, the paleouplift characteristics were obvious. After the late Cambrian, the Caledonian and Hercynian tectonic moved as the crust uplifted, the land was expanding resulting in an uplifted central Sichuan under water and gradually growing out of the sea surface. Such movement caused the overlying Ordovician, Silurian, Devonian and Carboniferous strata of the Longwangmiao Formation in the west part of the Basin lost or partially denudated, leading to the final formation of paleouplift. The Yanshan-Himalayan faulting activities were not violent, causing no damage or a little damage to
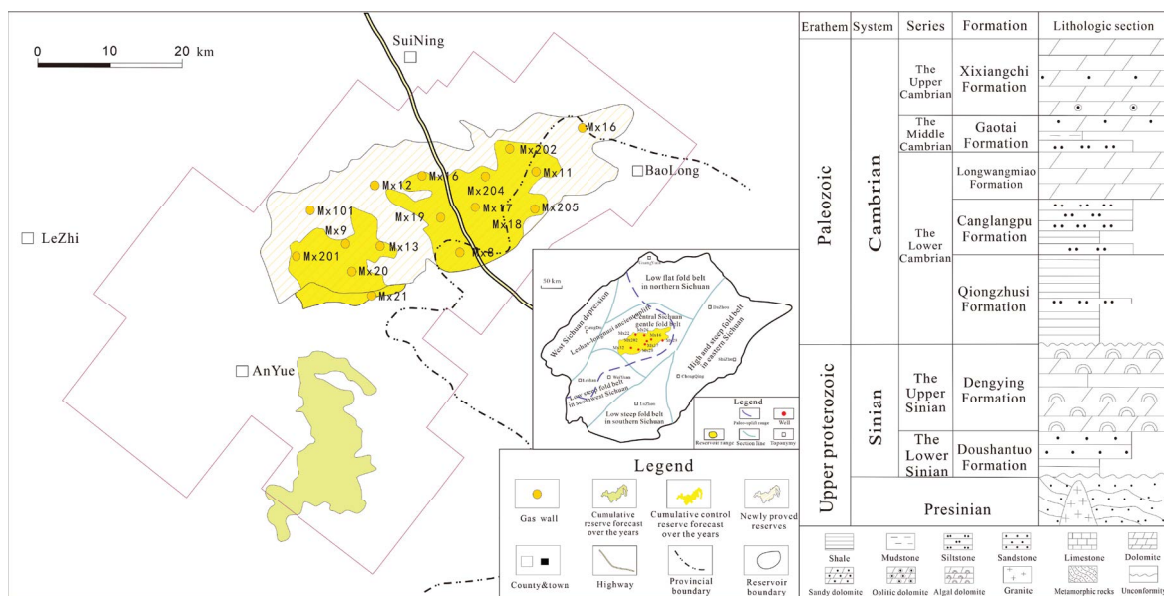

Fig. 1. Location, structure and stratigraphic column of MX area.

the ancient gas reservoir. Since then, the Longwangmiao Formation has been buried deep in the middle-deep environment despite structural adjustment [14–19]. The strata have extremely low terrain with a dip angle of 1°~6°.

3. Description of the original gas–water distribution of the gas reservoirs

3.1. Reservoir mode and characteristics of the formation water

3.1.1. General reservoir mode of the formation water in water-bearing gas reservoirs

Formation water in water-bearing gas reservoirs of structural trap are generally existing in three types which are bottom water, edge water and locally sealed water. Bottom water refers to the formation water at the bottom of the gas layer and supports natural gas [20]. The gas reservoir with bottom water due to insufficient natural gas filling has uniform gas–water interface and its gas–water interface intersects with the gas layer only [21]. Affected by physical properties and pore structures, the second type has gas–water transition areas of different thickness, as shown in Fig. 2a. The bottom water with sufficient energy often advances upward through the uneven forms of faulting systems, fractures, pores and other channels with different seepage capacity. Edge water refers to the formation water gathered in the lower part of the structure (such as the anticline wing) and surrounded natural gas from the edges of the gas layer [20]. In the third type, gas–water interface contacts the top and bottom of the gas layer, forming an interface where there are transition areas of a certain thickness, as shown in Fig. 2b. In general, the gas reservoir with edge water has a uniform gas–water interface, and edge water wells producing formation water are located in the lower structure of the gas reservoirs boundary. When developing, the pressure of edge water wells decreases as the production of adjacent gas wells increases, and the gas wells adjacent to edge water experiences water flooding during the production, which is the trait of edge water invasion [21]. Locally sealed water is often found in carbonate gas reservoirs, commonly known as "pocket water" or "lens water" with limited water energy [22,23]. Locally sealed water is developed because: (1) The formation water was retained as oil and gas are not discharged smoothly during the transportation caused by the physical property differences of the strata longitudinally, resulting in the formation of locally sealed water between the layers. (2) Locally physical property difference traps were formed due to horizontal changes in lithology

and physical properties. (3) Water is stranded in lower areas where the structure is low and gentle structure, leading to local stranded formation water, as shown in Fig. 2c.

3.1.2. Reservoir mode of the formation water of the Longwangmiao Reservoirs

Oil test is an important approach to establish the identification standard of gas reservoir fluids and reveal the gas–water relationship. According to more than 50 wells' oil tests results, the research area in the Longwangmiao Reservoirs consists of large gas areas and a large gas–water transition area where the edge water widely developed in the north and south wings of the gas reservoirs. The transition area is different from the one formed by the sufficient gas–water differentiation in regular gas reservoir with bottom water. The two types of transition areas are different but also have properties in common [10]. Tops of both transition areas are pure gas layers, while the central parts store gas and water, and pure water is extracted from the bottom. As for the difference, the transition area of the Longwangmiao Reservoirs is widely distributed and close to the gas area with good gas-bearing property. The oil test showed that Longwangmiao Reservoir transition area has less layers producing both gas and water as they are highly differentiated. Therefore, we classify the area above the gas–water interface of the target interval into pure gas area, the area below the gas–water interface into pure water area, and the area between the two as transition area. Meanwhile, due to the large-scale low and gentle structure, microstructure changes control the differential distribution of confined water as there is gas in the majority of the trap area. Such structure would easily form locally sealed water with non-uniform gas–water interface in locally low areas. To sum up, the storage mode of the formation water in the study area is mainly edge water with locally sealed water, as shown in Fig. 3.

3.2. Determination method of the original gas–water interface

3.2.1. Determination of the original gas–water interface based on the relationship between water saturation and elevation of the gas reservoirs (FL_0)

In the same pressure system, the saturation at the gas–water interface is equal in the original state. According to this principle, based on the exploration wells that can reflect the original gas–water properties of the research area, we make the relationship curve illustrating the correlation between water saturation of gas wells, water wells and their
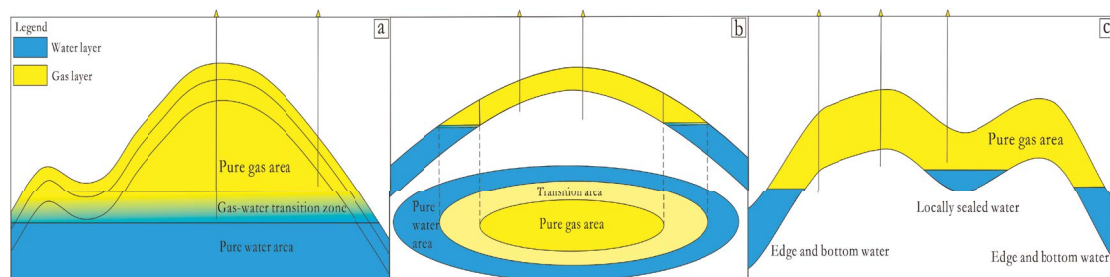

Fig. 2. Reservoir mode of the formation water.

corresponding elevation, so the intersection of the two curves represents the altitude of the gas–water interface [24]. The gas wells used to draw the curve are MX201, MX102, MX13, MX12, MX19 and MX17 and water wells are MX204 and MX47. Benchmarking against the water saturation of each well interpreted by logging, the research calculates the water saturation and its corresponding elevation of the effective reservoir both at the bottom and on the top of gas wells of the Longwangmiao Formation. Table 1 shows the detailed information of each well. By identifying the relationship between water saturation of gas wells and water wells considering their corresponding elevation respectively (Fig. 4), the gas–water interface of the gas reservoirs is preliminarily determined to be at –4,383 m.

3.2.2. Determination of the gas–water interface based on saturation-height modeling

Early well logging interpretation and oil test results showed that the gas reservoir does not have a uniform gas–water interface. For example, the gas–water interface of MX204 in the north wing of the main area is –4,385.4 m, MX203 in the south wing –4,392.8 m, and MX008-7-H1 in a low area –4,369 m. Therefore, it is necessary to use the mercury pressure data to establish the block saturation-gas column height model to calculate the exact optimal gas–water interface of each well, and ultimately describe the original gas–water distribution in the study area.
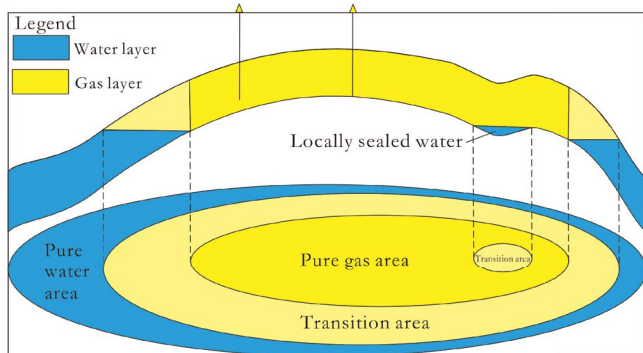

Fig. 3. Reservoir mode of the formation water of the Longwangmiao Reservoirs.

Table 1
Information of water saturation and elevation of data well collection points

Well no.	Sw (%)	H (m)
MX201	2.38	–4,299.55
MX102	16.394	–4,349.36
MX13	29.646	–4,354.82
MX12	21.595	–4,353.62
MX19	9.419	–4,338.77
MX17	29.68	–4,359.8
MX204	85.41	–4,385.38
MX47	99.9	–4,396.87

3.2.2.1. Water saturation model based on mercury pressure data

Mercury pressure data can effectively reflect the pore structure of the reservoir [25]. Under the balanced capillary pressure, the fluid saturation can be calculated based on the corresponding capillary pressure. Accordingly, this paper establishes the water saturation model for multiple core domains such as J function based on capillary pressure data.

3.2.2.1.1. Leverett-J function

The value of J function is related to porosity, permeability and capillary pressure, while other parameters are fixed values. The function shows that the capillary pressure curve changes with elevation [26]. Accordingly, the water saturation can be calculated based on the capillary pressure and physical parameters of the reservoir at different depths. The equation is:

$$S_w = a \times J^b + S_{wb} \tag{1}$$

$$J = \sqrt{k/\Phi} \times \frac{PC}{\sigma \cos \theta} \tag{2}$$

where S_w is the water saturation, %; a, b are the regression constants; S_{wb} is the comparison expression related to pore seepage generated by fitting; J is the J function, non-dimensional number; P_C is the capillary pressure, MPa; σ is the interface tension, Mn/m; θ is the wetting angle, (°); K is the permeability, mD; Φ is the sample porosity, %.

3.2.2.1.2. Brooks-Corey equation

The Brooks-Corey model demonstrates the quantitative relationship between water saturation and capillary pressure in gas–water two-phase [27], which can be applied to three-phase fluids. The equation is:

$$S_w = S_{wb} + \left(1 - S_{wb}\right) \times \left(\frac{P_{Ce}}{P_C}\right)^{1/n} \tag{3}$$
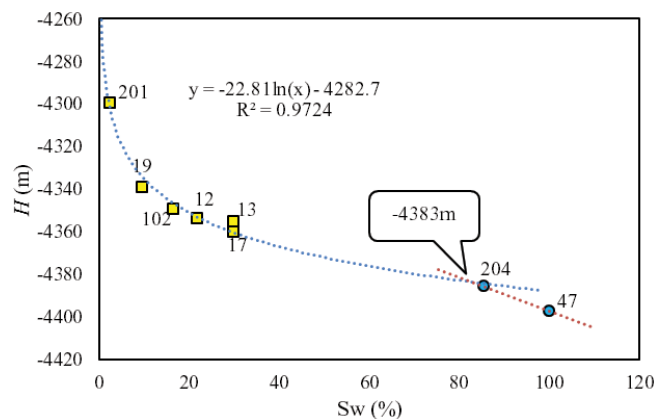

Fig. 4. Relationship curve between water saturation of gas wells and water wells and corresponding elevation.

where S_w is the water saturation, %; S_{wb} and n are the comparison expressions related to pore seepage generated by fitting; P_C is the capillary pressure, P_{Ce} is the threshold pressure, MPa.

3.2.2.1.3. Lambda equation

The Lambda model can efficiently describe the capillary pressure curve shape [28], and get better fitting results in the capillary pressure curve fitting. The equation is:

$$S_w = A \times P_C^{-\lambda} + b \tag{4}$$

where S_w is the water saturation, %; A and λ are the comparison expression related to pore seepage obtained by fitting; P_C is the capillary pressure, MPa; b is the regression constant.

3.2.2.1.4. Thomeer equation

The bilogarithmic coordinates of the intersection of the incoming mercury pressure and the capillary pressure show a mathematical hyperbolic relationship [29,30]. Based on the equation of the hyperbola proposed by Thomeer built the water saturation calculation model. The equation is:

$$S_w = S_{wb} + \left(1 - S_{wb}\right) \times \left(1 - e^{\left(G/\ln\left(P_{Ce}/P_C\right)\right)}\right) \tag{5}$$

where S_w is the water saturation, %; S_{wb} and n are the comparison expression related to pore seepage obtained by fitting; P_C is the capillary pressure; P_{Ce} is the threshold pressure, MPa; G is the pore geometrical factor describing the degree of crook of the capillary pressure curve and reflecting the morphology of the pore throat.

3.2.2.2. Calculation of the optimal gas–water interface

Assuming that the logging interpretation is reliable and conforms to the actual gas reservoir, the water saturation continuous curve (S_{w0}) calculated based on the logging curve is substituted into the above four equations. The optimized parameters of the water saturation model of the core domain will then optimize the water saturation model of the logging domain. Subsequently, we calculated the water saturation continuous curve of logging domain (S_{w1}). The universal function relationship based on S_{w0} interpreted by the well-logging, porosity (ϕ), permeability (K) and the initial free water surface FL_0 (–4,383 m) determined according to Fig. 4 is established by adopting the least square method, namely: $S_w = f\ (FL, \phi, K)$.

If the initial free water surface FL_0 is not consistent with the actual gas reservoir, by comparing the continuous saturation curves S_{w0} and S_{w1}, both hanging with depth, we found that the elevation becomes the optimal free water surface when the difference between the two curves reaches the minimum value. The Nelder-Mead algorithm is used to solve this extreme value problem, which requires no differentiable functions and converges to a local minimum more quickly. The optimized saturation-gas column height model calculated the optimal gas–water interface of MX203, a well explored earlier, in the gas reservoir (Table 2). The four methods are basically consistent, with an average interface elevation of –4,395.1 m, consistent with the test-confirmed gas–water interface at –4,392.8 m. The results indicate that the model is reliable and can be applied to the remaining wells in the study area.

The calculation results of the optimal free water surface of multiple key formation penetrating wells in the area are shown in Table 3. According to Table 3, the main area

Table 2
Calculation results of water saturation-height model of MX 203

Well no.	Water saturation-height model	Sounding (m)	Elevation (m)
MX203	Brooks-Corey	4,768.261	–4,395.2
	Lambda	4,768.369	–4,395.3
	Thomeer	4,768.369	–4,395.3
	Leverett-J	4,767.365	–4,394.5

Table 3
Calculation results of water saturation-height model in the entire well area of the Longwangmiao Formation

Well area	Well no.	Brooks-Corey		Lambda		Thomeer		Leverett-J	
		Sounding	Elevation	Sounding	Elevation	Sounding	Elevation	Sounding	Elevation
MX9 area	MX102	4,733.2 m	–4,385.8 m	4,731.5 m	–4,384.1 m	4,730.9 m	–4,383.5 m	4,731.5 m	–4,384.1 m
	MX101	4,710.7 m	–4,397.2 m	4,702.3 m	–4,388.7 m	4,698.6m	–4,384.9m	4,670.3m	–4,386.5m
	MX116	4,705.5 m	–4,392.1 m	4,712.1 m	–4,399 m	4,705.5 m	–4,392.3 m	4,698.3 m	–4,385.2 m
	MX9	4,711.5 m	–4,387.0 m	4,710.2 m	–4,385.7 m	4,710.2 m	–4,385.7 m	4,716.9 m	–4,392.4 m
	MX201	4,697.3 m	4,387.8 m	4,695.3 m	–4,385.7 m	4,698.4 m	–4,389.2 m	4,695.3 m	–4,385.7 m
	MX118	4,698.8 m	–4,385.2 m	4,700.9 m	–4,387.3 m	4,699.7 m	–4,386.2 m	4,706.3 m	–4,392.5 m
	MX8	4,733.1 m	–4,393.4 m	4,733.3 m	–4,393.5 m	4,733.4 m	–4,394.6 m	4,733.3 m	–4,393.5 m
	MX18	4,696.2 m	–4,392.5 m	4,692.7 m	–4,389.2 m	4,698.9 m	–4,395.3 m	4,692.8 m	–4,388.5 m
MX8 area	MX205	4,678.9 m	–4,414.4 m	4,677.9 m	–4,413.3 m	4,679.3 m	–4,415.1 m	4,680.8 m	–4,416.2 m
	MX10	4,730.8 m	–4,408.9 m	4,731.8 m	–4,410.1 m	4,729.9 m	–4,407.9 m	4,730.9 m	–4,408.7 m
	MX19	4,737.7 m	–4,384.9 m	4,737.6 m	–4,384.8 m	4,738.2 m	–4,385.4 m	4,735.0 m	–4,382.6 m

of Longwangmiao Reservoirs has no uniform gas–water interface. The gas–water interface in the north wing changes within the range of –4,385 ± 3 m while the interface in the south wing varies –4,390 ~ –4,410 m, lower than the north wing.

3.3. Fin and detailed description of the original gas–water distribution of the gas reservoirs

According to the above calculation, if the structural contour line is lower than the optimal gas–water interface in the well area, the region will be classified as pure water are, while the pure gas area refers to the zone where the bottom interface of the reservoir section is higher than the optimal gas–water interface. Between the pure water area and the pure gas area lies the transition area. The boundary between the pure gas area and the transition area is determined by the difference value between the bottom elevation of the target stratum and the gas–water interface of the well, as shown in Table 4. Fig. 5 illustrates the original gas–water relationship distribution in the study area. The pure gas areas are located at an elevation above –4,320 m of the northern structural contour of MX9 and MX8 areas, and above –4,310 m in the south of MX8 area. Natural gas is widely distributed in the main area, controlled by the structural trap of the main area. There is a wide transition area between the edge water and the pure gas. In the north wing, there is a flat structure and wide transition area, but the south wing has steep structure, and the transition area is narrow.

4. Dynamic change law of the gas–water distribution

During the development of water-bearing gas reservoirs, water discharging from gas wells caused by water invasion will not only make the exploitation more difficult, but also cause capacity loss to the gas production, slowing

the recovery of gas reservoirs and profitability. Therefore, to develop the gas reservoirs effectively, it is necessary to clarify the reservoir characteristics and identify the dynamics of water invasion [31].

4.1. Reservoir classification and plane distribution pattern

Microscopic pore structure is a decisive factor in identifying the reservoir permeability and accumulating oil and gas reservoirs. It is also the core at the study on the reservoirs' microphysical characteristics, directly affecting the storage capacity and seepage capacity of reservoirs [32]. Therefore, analyzing the microscopic pore structure characteristics and comprehensive property parameters is an important way to study the reservoir quality in the research of the Longwangmiao Reservoirs. The pore structures of the reservoir are analyzed with mercury pressure data, the reservoirs of similar pore throat structures are grouped into one category. Thus, the reservoirs in the study area are divided into three categories, as shown in Fig. 6.

4.1.1. Type I reservoir

It is considered to have the best properties in the study area. The analysis of mercury pressure experimental samples showed that apertures of Type I reservoir are concentrated in the range of 2 ~ 20 m with well throat sorting. The core sample porosity of the reservoir is greater than 5.5% with permeability greater than 0.25×10^{-3} μm^2, which reflect high liquidity of the reservoir. The wells in Type I reservoir have high and stable productivity.

4.1.2. Type II reservoir

The quality of Type II reservoir is considered is next to the best in the study area. Comparing with Type I reservoir,

Table 4
Calculation results of the depth between target section and gas–water interface of formation penetrating wells

| Well no.	Bottom elevation of the objective interval	Optimal gas–water interface elevation	Depth difference between the objective interval and gas–water interface
MX102	–4,364.2 m	–4,385.8 m	21.6 m
MX101	–4,352.3 m	–4,389.3 m	37.0 m
MX116	–4,394.5 m	–4,392.2 m	–2.3 m
MX13	–4,369.5 m	–4,384.8 m	15.3 m
MX9	–4,315.7 m	–4,392.2 m	76.5 m
MX201	–4,320.6 m	–4,387.6 m	67.0 m
MX118	–4,326.4 m	–4,387.8 m	61.4 m
MX203	–4,433.7 m	–4,396.1 m	–37.6 m
MX20	–4,344.8 m	–4,385.0 m	40.2 m
MX8	–4,394.4 m	–4,393.8 m	–0.6 m
MX18	–4,389.9 m	–4,391.4 m	1.5 m
MX205	–4,410.5 m	–4,414.8 m	4.3 m
MX17	–4,363.8 m	–4,381.4 m	17.6 m
MX204	–4,439.9 m	–4,385.0 m	–54.9 m
MX10	–4,405.3 m	–4,408.9 m	3.6 m
MX12	–4,365.7 m	–4,379.7 m	14.0 m
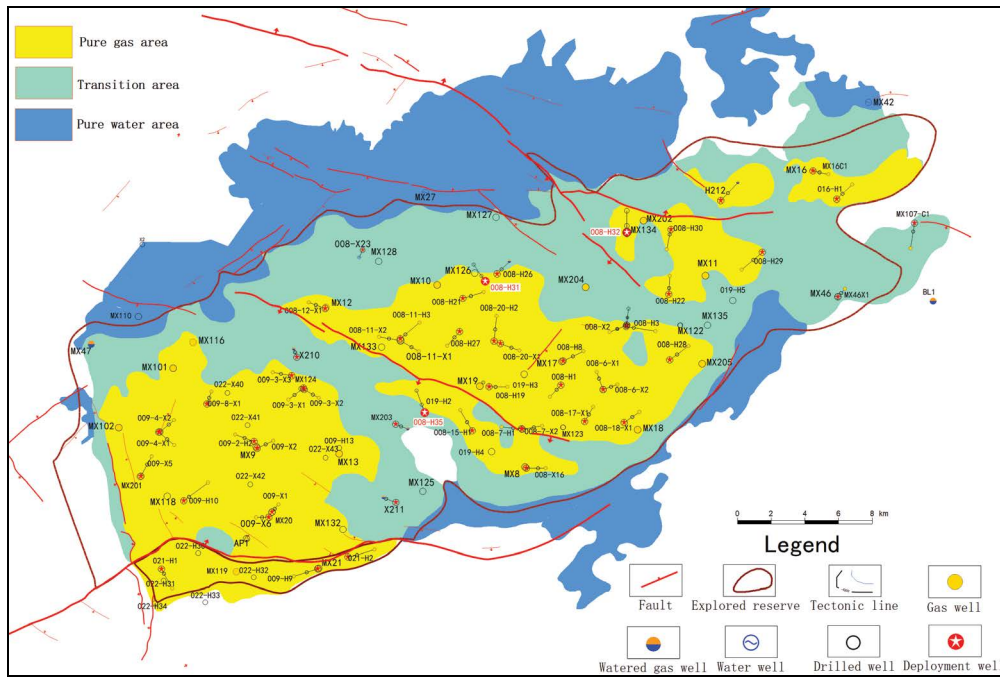
Fig. 5. Distribution diagram of the original gas–water relationship of the Longwangmiao Reservoirs.
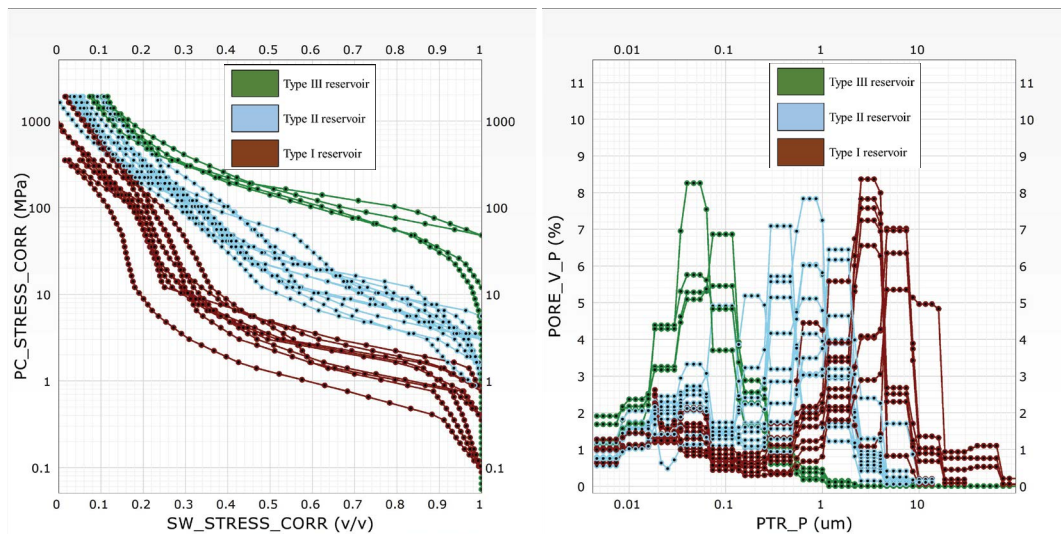

Fig. 6. Capillary pressure curve (a) and pore size distribution (b) in the main area of the Longwangmiao Formation in MX gas field.

apertures of this reservoir are concentrated between 0.1 ~ 2 m with slightly worse pore throat sorting. The core sample porosity of the reservoir is generally ranging 3.3% ~ 5.5% with permeability of $0.015 \times 10^{-3} ~ 0.25 \times 10^{-3}$ μm². The overall performance of Type II reservoir shows that the initial productivity is good, but less stability than that of Type I reservoir.

4.1.3. Type III reservoir

Type III reservoir has the worst quality in the study area. Compared to the first two types, apertures of this type are concentrated at 0.01 ~ 0.1 m, representing a fine-micropore and small throat structure. The core sample porosity is generally less than 3.3%, with permeability less than 0.015×10^{-3} μm².

The whole region classification is based on the above reservoir classification criteria (Fig. 7). The distribution pattern can be concluded as: MX9 area is mainly developed with Type II reservoir, among which MX116 and MX101 in the north Type III reservoir, MX9 and MX13 in the middle high quality Type I reservoir, and MXX211 in the south Type III reservoir. MX8 area has relatively poor reservoir with wide development of Type III reservoir, among which MX126 in
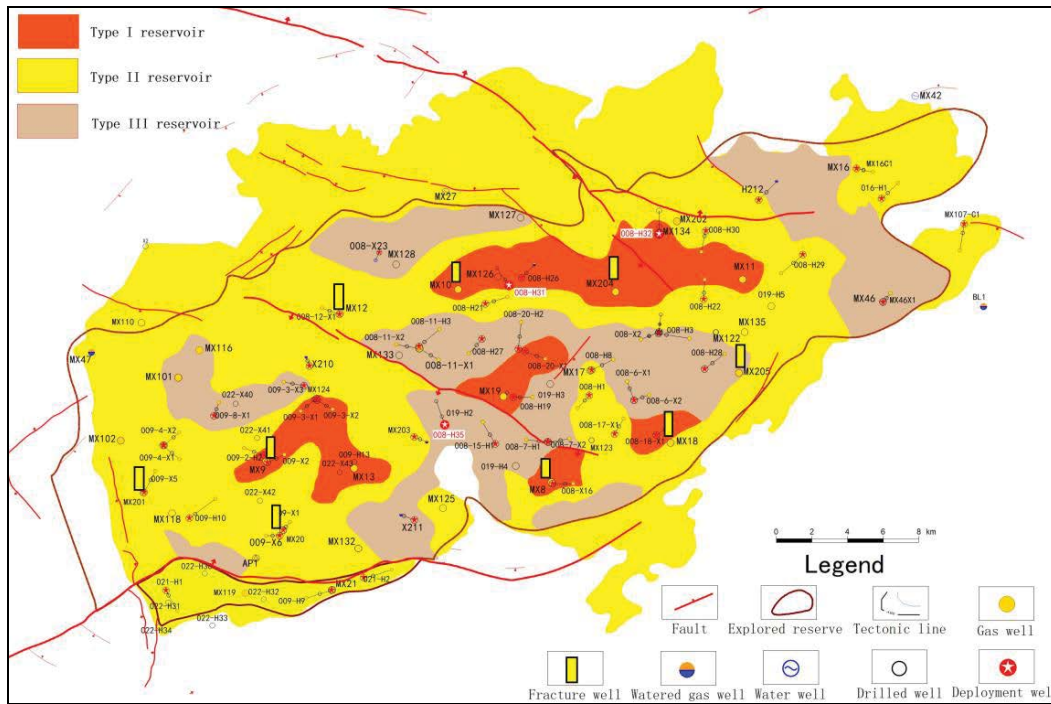
Fig. 7. Classification plan of the Longwangmiao Reservoirs.

the north wing is mainly developed with Type III reservoir, MX204 in the east Type I reservoir, MX8 and MX18 in the south Type I reservoir. According to the relationship between reservoir thickness and test yield (Fig. 8), some wells with poor matrix physical properties but good fracture development have high productivity, indicating that single well yield is related not only to the development of fractures but also the control of reservoir types.

4.2. Water invasion behaviors and paths

According to the above analysis, the seepage capacity of the gas reservoirs and the water invasion behaviors of the formation water are mainly affected by the reservoir type and the fracture development degree. Combined with the dynamic data of gas reservoir production, we identified a total of 7 advantage water invasion channels, as shown in Fig. 9. Among them, there are three channels in MX9 area: (1) From MX102 to the inside of the gas reservoirs; (2) From MX009-8-X1 to the inside of the gas reservoirs; (3) Well Group MX009-3 to the inside of the gas reservoirs. There are four channels in MX8 area: (1) from the southwest wing of MX8 to the inside of the gas reservoirs; (2) from the southwest wing of MX18 ~ 205 area to the inside of the gas reservoirs; (3) from MX008-H26 ~ 204 to the inside of the gas reservoirs; (4) from MX12 to the inside of the gas reservoirs.

4.3. Change pattern of gas–water distribution

The water invasion speed and the uplifting height of gas–water interface are inferred based on the analysis of reservoir quality, fracture development and water invasion channels, as well as on the production dynamic data. Thus,
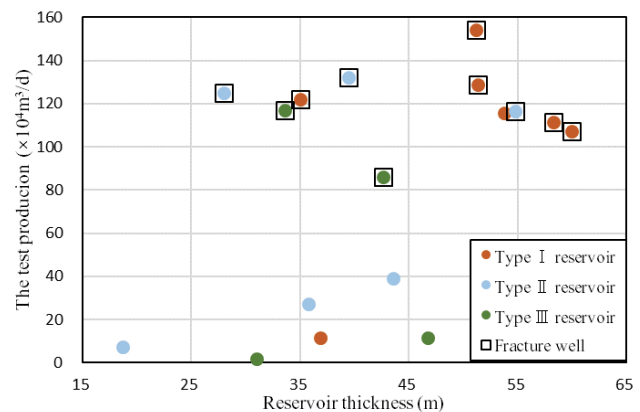

Fig. 8. Cross-plot of the test production corresponding to the thickness of various reservoirs in the main area.

the gas–water distribution of the Longwangmiao Reservoirs in 2021 is drawn according to the original gas–water distribution (Fig. 9). Comparing with the original gas–water distribution, the gas–water interface is advancing non-uniformly rapidly along the high permeability zone and fracture development area of Type I reservoir during the development.

4.3.1. MX9 Zone

- *North of MX9 Zone in the main area*: MX102 is invaded by water. It is speculated that the gas–water interface rises by about 20 m, while MX47 is completely flooded by water in the pure water area. The reservoir quality of MX101 and MX116 is poor as the gas–water interface rises slowly.
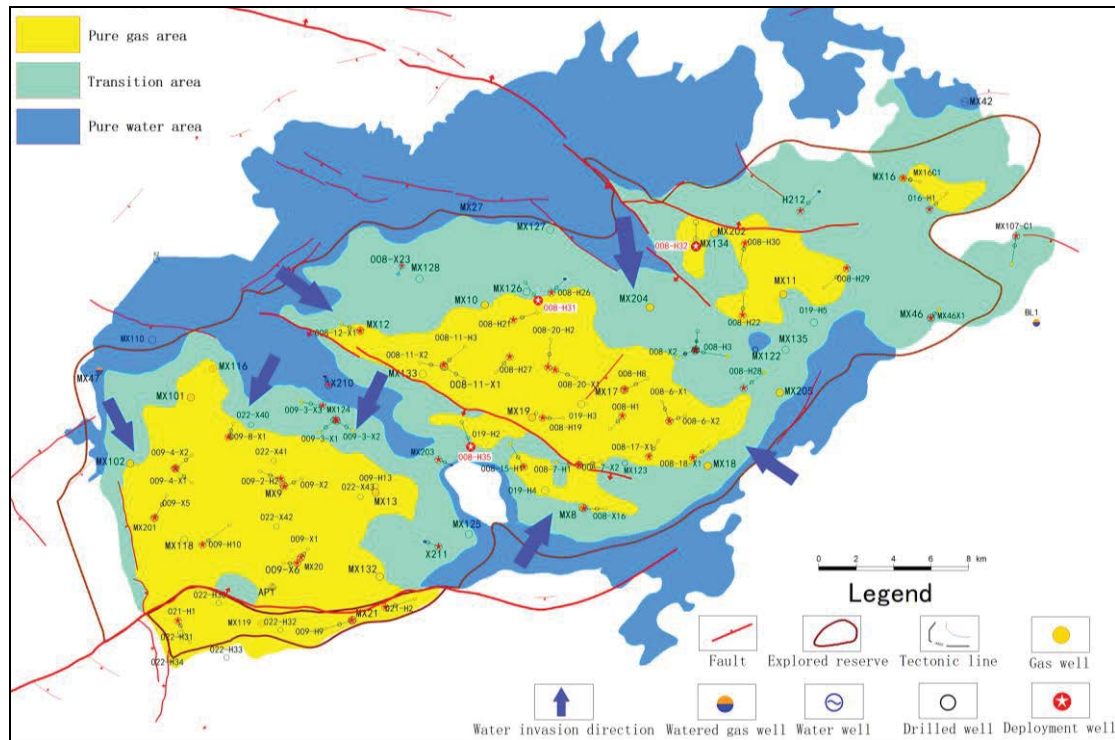
Fig. 9. Gas and water distribution map of the Longwangmiao Formation in MX gas field (2021).

- *East of MX9 Zone in the main area*: Well Group MX009-3 is located in the transition area. The logging interpretation of the newly completed MX124 shows that the gas–water interface in the area rises by about 65 m.
- *South of MX9 Zone in the main area*: the gas–water interface analysis of logging interpretation of the newly completed MX125 and MXX211 shows that the gas–water interface in the area rises slowly but remains at around –4,385 m.

4.3.2. MX8 Zone

- *North of MX8 Zone in the main area*: MX008-12-X1, located in the transition area in the north, has been flooded by water, with gas–water interface rising by around 30 m. MX12 is still in the pure gas area. The newly completed MX128 shows that the gas–water interface rises slowly in this area at around –4,384 m.
- *East of MX8 Zone*: the production dynamics of MX008-H3, MX008-X2 and MX008-H28 show that it is producing water as the gas–water interface lifting about 30 m in the transition area.
- *South of MX8 Zone in the main area*: MX18 and MX205 show strong water seepage capacity due to fracture development, as the gas–water interface rises by about 50 m and transition area expands. As MX8 has been in the gas–water transition area, it is speculated that the gas–water interface rises by about 40 m. The logging interpretation of the newly completed MX019-H2 and MX019-H4 shows that the wells are still in the pure gas area.

5. Conclusion

- According to the change value of water saturation of water and gas wells against the elevation depth, the gas–water interface is determined to be at the depth near –4,383 m. The Leverett-J function, Brooks-Corey equation, Lambda equation and Thomeer equation help establish a water saturation-height model to calculate the optimal gas–water interface, thus describing the original gas–water distribution of the gas reservoirs in detail. It is believed that the original gas–water interface of the gas reservoirs is not uniform, while the water interface in the north wing of the main area changing within –4,385 ± 3 m, but the gas–water interface of the south wing changes greatly within –4,390 ~ –4,410 m due to the influence of dip angle and water energy.
- The Longwangmiao Reservoirs are divided into three categories by the seepage capacity with strong heterogeneous characteristics. Type I reservoir has the best properties in the study area with stable and high productivity.
- Due to multiple factors such as structure, lithology, pore throat structure difference, fracture development extent and coexistence of various formation water reservoir modes, the gas–water interface rises non-uniformly during the development. The reservoir division and fracture analysis identified seven water invasion paths, among which three are in MX9 area and four in MX8 area. Production dynamics show that the water in the main area is advancing rapidly along the high permeability zone and fracture development area of Type I reservoir.

References

[1] L. Tan, H. Liu, Y.Z. Tang, F. Li, Q.S. Tang, F. Liang, M. Li, W. Liu, Reservoir characteristics and seismic response of the Longwangmiao Formation of Longnvsi structure in Sichuan Basin, Nat. Gas Geosci., 31 (2020) 1802–1813.

[2] X.M. Lin, H.F. Yuan, L.Q. Zhu, W. Zeng, Y.Q. Xu, Hydrocarbon accumulation history of the Cambrian Longwangmiao Formation in the Anyue structure of the central Sichuan Basin, Acta Geol. Sin., 94 (2020) 916–930.

[3] J.G. Zhou, C.C. Xu, G.S. Yao, G. Yang, J.Y. Zhang, Y. Hao, F. Wang, L.Y. Pan, M.F. Gu, W.Z. Li, Genesis and evolution of Lower Cambrian Longwangmiao Formation reservoirs, Sichuan Basin, SW China, Pet. Explor. Dev., 42 (2015) 175–184.

[4] X.Z. Li, Z.H. Guo, Y.J. Wan, X.H. Liu, M.L. Zhang, W.R. Xie, Y.H. Su, Y. Hu, J.W. Feng, B.X. Yang, S.Y. Ma, S.S. Gao, Geological characteristics and development strategies for Cambrian Longwangmiao Formation gas reservoir in Anyue gas field, Sichuan Basin, SW China, Pet. Explor. Dev., 44 (2017) 428–436.

[5] K. Sun, K. Xu, Q.H. Chen, Characterization and application of structural fracture length in low permeability reservoir: a case study of Cambrian Longwangmiao Formation in Moxi-Gaoshiti area, Sichuan Basin, Pet. Geol. Exp., 44 (2022) 160–169.

[6] G.R. Zhang, Q. Liao, Y. Yu, Q. Ran, Y. Xiao, X.M. Lu, H. Liang, M. Zeng, Seismic prediction on the favorable efficient development areas of the Longwangmiao Fm gas reservoir in the Gaoshiti–Moxi area, Sichuan Basin, Nat. Gas Ind., 37 (2017) 66–75.

[7] Y.P. Wang, X.F. Yang, X.Z. Wang, Z.S. Huang, C. Chen, Y.M. Yang, W.J. Luo, Reservoir properties and genetic mechanism of grain dolomite of the Longwangmiao Formation, Moxi area in central Sichuan Basin, Geol. Sci. Technol. Inf., 38 (2019) 197–205.

[8] C. Xi, Y. He, Y. Liu, Y. Li, X.L. Bai, S.H. Wu, H. Li, Seismic response characteristics of the Lower Cambrian Longwangmiao Formation reservoirs in the eastern Sichuan Basin, Nat. Gas Ind., 40 (2020) 39–46.

[9] X.H. Zhang, W.J. Luo, L. Wen, B. Luo, H.L. Peng, M.L. Xia, Sedimentary facies evolution characteristics and petroleum geological significance of Cambrian Group in Sichuan Basin, Fault Block Oil Gasfield, 25 (2018) 419–425.

[10] C. Zhang, X. Peng, Q. Li, B. Wang, H.X. Guo, Fine description on gas–water distribution for carbonate-rock gas reservoirs in large-scale low and gentle structures: an example from the Longwangmiao Formation, Moxi block, Sichuan Basin, Nat. Gas Explor. Dev., 42 (2019) 49–57.

[11] B. Wang, C.C. Yang, Y.Y. Li, C. Zhang, Study on Gas–Water Distribution Characteristics of Deep Heterogeneous Gas Reservoirs: A Case From Gas Reservoir of the Longwangmiao Formation in Moxi Area, Sichuan Basin, 2018 The National Gas Academic Essays (02) Gas Pool Development, 2018, pp. 69–75.

[12] C.N. Zou, J.H. Du, C.C. Xu, Z.C. Wang, B.M. Zhang, G.Q. Wei, T.S. Wang, G.S. Yao, S.H. Deng, J.J. Liu, H. Zhou, A. Xu, Z. Tang, H. Jiang, Z.D. Gu, Formation, distribution, resource potential, and discovery of Sinian–Cambrian giant gas field, Sichuan Basin, SW China, Pet. Explor. Dev., 41 (2014) 306–325.

[13] W.Q. Yang, Z. Liu, H.R. Chen, C.J. Lan, Z.H. Xu, C.J. Lu, H.Y. Zou, The grain beach sedimentary assemblages of Lower Cambrian Longwangmiao Formation in Sichuan Basin and their controlling effects on reservoirs, J. Palaeogeogr., 22 (2020) 251–265.

[14] B. Hao, W. Zhao, S.Y. Hu, S.Y. Shi, P. Gao, T.S. Wang, S.P. Huang, H. Jiang, Bitumen genesis and hydrocarbon accumulation history of the Cambr-ian Longwangmiao Formation in Central Sichuan Basin, Acta Pet. Sin., 38 (2017) 863–875.

[15] J.H. Du, C.N. Zou, C.C. Xu, H.Q. He, P. Shen, Y.M. Yang, Y.L. Li, G.Q. Wei, Z.C. wang, Y. Yang, Theoretical and technical innovations in strategic discovery of a giant gas field in Cambrian Longwangmiao Formation of central Sichuan paleo-uplift, Sichuan Basin, Pet. Explor. Dev., 41 (2014) 294–305.

[16] C. Zhang, C.C. Yang, Y.C. Liu, X.F. Yang, B. Wang, Z.M. Zhu, Controlling factors of fluid distribution in the lower Cambrian Longwangmiao Formation, Moxi area, Sichuan Basin, Geol. Explor., 53 (2017) 599–608.

[17] K. Ma, P. Shen, Z.C. Wang, X.W. Tian, H.L. Peng, H. Wang, X.H. Zhang, Y.T. Sun, B. Luo, Y.L. Wang, D.L. Yang, Natural gas exploration potential of the Longwangmiao Formation on the north slope of Chuanzhong paleo – uplift from the characteristics of "Four Paleo", Nat. Gas Geosci., 30 (2019) 1451–1464.

[18] D.W. Liu, C.F. Cai, Y.J. Hu, L. Jiang, Y.Y. Peng, R. Yu, Q. Qin, Multi-stage dolomitization process of deep burial dolostones and its influence on pore evolution: a case study of the Longwangmiao Formation in the Lower Cambrian of central Sichuan Basin, J. China Univ. Min. Technol., 49 (2020) 1150–1165.

[19] T. Zhang, X.Z. Ma, W.W. Zhao, J.J. Fan, X.S. Lu, S.H. Yan, Characteristics of paleo-oil reservoir of the Longwangmiao Formation in Moxi-Gaoshiti Area, Fault-Block Oil Gasfield, 24 (2017) 466–470.

[20] G.D. Liu, Petroleum Geology, Petroleum Industry Press, Beijing, 2009.

[21] C. Cheng, Y. Wei, J. Huang, S.Q. Hu, C.L. Wu, A.H. Zhang, Study on formation water storage mode of carbonate reservoir with water in southern Sichuan area, J. Yangtze Univ. (Nat. Sci. Ed.), 9 (2012) 51–54.

[22] D.H. Wu, Q. Sang, S.Y. Zhou, C.L. Wu, A.H. Zhang, Study on water invasion characteristics of Maokou Formation gas reservoir in Kongtan Gasfield, Nat. Gas Explor. Dev, 34 (2011) 54–56.

[23] R. Li, Characteristics and Genesis of Formation Water in the 2nd Member of Shan Formation in Yulinnan-Zizhou Area, Inner Mongolia Petrochemical Industry, 2008, pp. 95–96.

[24] M.S. Dong, Evaluation of Gas–Water Interface Determination Method for Carboniferous Gas Reservoirs in Zhangjiachang Gasfield, Eastern Sichuan, Natural Gas Industry, 1996, pp. 31–33+12–13.

[25] C. Wang, B. Pan, G. Chen, Evaluation of water saturation in low resistivity reservoir using mercury injection data, Well Logging Technol., 37 (2013) 166–168.

[26] B.X. Dai, X.Y. Fang, J.L. Huan, Y.J. Dai, Y.N. Gan, The establishment of offshore oilfield three-dimensional water saturation model by J function direct fitting method, J. Hebei GEO Univ., 40 (2017) 1–5.

[27] B. Hou, Acoustics simulation and analysis of three phase fluid patchy saturations porous rock, Scientia Sinica (Physica, Mechanica & Astronomica), 42 (2012) 259.

[28] G.W. Bi, Reservoir water saturation calculation by Lambda function method, Well Logging Technol., 40 (2016) 443–446.

[29] J.H.M. Thomeer, Introduction of a pore geometrical factor defined by the capillary pressure curve, J. Pet. Technol., 12 (1960) 73–77.

[30] C. Zhang, X. Tang, G.H. Ni, Y.Y. Min, Y.N. Zhang, Evaluation of carbonate reservoir permeability in Middle East Block based on Thomeer function, J. Yangtze Univ. (Nat. Sci. Ed.), 18 (2021) 43–51.

[31] S. Wang, K. Zhang, L.J. Chao, D.H. Li, X. Tian, H.J. Bao, G.D. Chen, Y. Xia, Exploring the utility of radar and satellite-sensed precipitation and their dynamic bias correction for integrated prediction of flood and landslide hazards, J. Hydrol. (Amsterdam), 603 (2021) 126964, doi: 10.1016/j.jhydrol.2021.126964.

[32] L. Wei, S.W. Ma, Z.L. Wang, Y.J. Wang, Static characterization and dynamic evaluation of micro-pore structure of carbonate reservoir: a case study of Ma5 Member in northwestern Ordos Basin, Mar. Origin Pet. Geol., 26 (2021) 131–140.